Precambrian Research 249 (2014) 100–114

Contents lists available at ScienceDirect

Precambrian Research

journal homepage: www.elsevier.com/locate/precamres

Structural and metamorphic evidence for Mesoarchaean subduction in the Finlayson Lake greenstone belt, Superior Province, Ontario

Nils R. Backeberg*, Christie D. Rowe, Vincent J. van Hinsberg, Eric J. Bellefroid

Department of Earth and Planetary Sciences, McGill University, Montréal, QC H3A 0E8, Canada

ARTICLE INFO

Article history:
Received 10 February 2014
Received in revised form 29 April 2014
Accepted 2 May 2014
Available online 24 May 2014

Keywords:
Superior Province
Marmion terrane
Archaean tectonics
Kinematics
Greenstone belt architecture

ABSTRACT

The unique structural architecture of Archaean terranes has generated competing models for early earth tectonics. Understanding the structural and metamorphic history of an individual terrane allows us to compare the deformation path to that predicted by tectonic models, and determine the best model for matching field observations. The Finlayson Lake greenstone belt is a Mesoarchaean terrane lying between three different gneiss terranes in the south-central Wabigoon subprovince in Canada. The belt has been interpreted as either a synformal keel sagducted between rising gneiss diapirs or as three fault-bounded allochtonous sub-belts of different ages. We present a detailed structural field study to define the deformation history of the Finlayson Lake greenstone belt and show that it is not consistent with either previous hypothesis. The Finlayson Lake greenstone belt is a single volcanic package that incorporates detritus from exposed felsic terranes similar in age and composition to the adjacent 3.0 Ga Marmion tonalites. The geometry of the greenstone belt is defined by two outward-facing palaeo way-up orientations (anticlinal) and geothermobarometry records a clockwise metamorphic path with a deep prograde event at 820 ± 40 MPa (27–30 km) and 600 ± 45 °C, followed by peak metamorphism at 635 ± 165 MPa (21–23 km) and 625 ± 25 °C. The deformation history records sinistral transpression during peak metamorphism and continued flattening during retrogression and exhumation from ductile to brittle regimes. The structural and metamorphic results are comparable with modern subduction-accretion style settings. The intensity of both retrogressive and brittle deformation fabrics during exhumation decrease from east to west away from the eastern boundary shear zone, the Marmion Shear Zone. Stronger deformation along the eastern margin of the Finlayson Lake greenstone belt, adjacent to the Marmion Shear Zone, suggest reactivation during exhumation and is likely related to the 2.7 Ga amalgamation of the Superior Province.

© 2014 Elsevier B.V. All rights reserved.

1. Introduction

The fundamental architecture of Archaean continental fragments worldwide is geometrically distinct from Proterozoic and Phanerozoic terranes, leading to various hypotheses for the processes of tectonics during this early part of Earth's history. In Archaean terranes, narrow belts of mafic volcanics, intrusives and sediments, usually metamorphosed at greenschist or low-amphibolite facies, are pinched between equant or elliptical domes of tonalite, trondhjemite, and granodiorite gneisses (TTGs), collectively known as TTG-greenstone terranes (e.g. Anhaeusser et al., 1969; Marshak et al., 1992; Percival and Helmstaedt, 2004; Percival, 2007a, and others). Archaean tectonics and crustal deformation have been addressed by various authors, generating a long-standing debate on when subduction-dominated tectonics took over from vertical diapiric tectonics (Fyson, 1978; Collins, 1989; Schwerdtner, 1990; Lin et al., 1996; de Wit, 1998; Hamilton, 1998; Chardon et al., 1998; Zegers and van Keken, 2001; Van Kranendonk et al., 2004; van Hunen et al., 2008; Kusky et al., 2014). Geometrically different interpretations of the inter-TTG greenstone belts support the different tectonic models, either accretionary terranes from collision-style tectonics (e.g. Sleep and Windley, 1982; Card, 1990; Calvert et al., 1995; Kusky and Vearncombe, 1997; Polat et al., 1998; Percival et al., 2004) or as synformal keels sinking or "sagducting" between rising TTG gneiss diapirs (Schwerdtner, 1984; Minnett and Anhaeusser, 1992; Robin and Bailey, 2009). The kinematic signature and deformation history of exposed greenstone belts and adjacent TTG domes should allow us to test these tectonic settings for a given Archaean terrane, by interpreting belt-scale architectures from detailed structural studies. The strongest observational evidence for synformal greenstone belts as a result of sagduction during diapiric tectonics comes from structural studies in the Australian Pilbara craton, which show strong flattening fabrics parallel to the greenstone belt margins and steep stretching

* Corresponding author. Tel.: +1 514 398 6767; fax: +1 514 398 4680.
E-mail address: nils.backeberg@mail.mcgill.ca (N.R. Backeberg).

http://dx.doi.org/10.1016/j.precamres.2014.05.012
0301-9268/© 2014 Elsevier B.V. All rights reserved.

lineations in the centre of the belt (eg Collins and Teyssier, 1990; Collins et al., 1998). This architectural model has been adopted for parts of the Superior Province in Canada without the same level of detailed kinematics from greenstone belt field studies.

Thorough kinematic studies on Superior Province Archaean terranes are rare (exceptions include Borradaile and Schwerdtner, 1984; Lin et al., 1996; Polat and Kerrich, 1999; Lin, 2005; Parmenter et al., 2006). Our contribution focusses on the Mesoarchaean Finlayson Lake greenstone belt (hereafter referred to as the Finlayson belt), which was deposited over a period of at least 70 million years between 2.93 Ga and 3.00 Ga (Davis and Jackson, 1988; Thomlinson et al., 1999, 2003; Stone, 2010). The Finlayson belt is located in the Marmion terrane of the south-central Wabigoon subprovince of Superior Province (see Fig. 2 in Percival, 2007b, for regional context). Three TTG gneiss domes of similar ages border the Finlayson belt: the 3.00 Ga Marmion gneiss; the 2.93 Ga Dashwa gneiss; and the 2.94 Ga Hardtack gneiss (Fig. 1a) (see Stone, 2008). The lithologies of the Finlayson belt are dominated by basaltic lava flows, pillow basalts and include finely laminated clastic and chemical sediments, siltstones and graded sandstones with minor conglomerates (Stone, 2008, 2010). All depositional contacts are tilted to sub-vertical and strike approximately northeast, parallel to the eastern boundary with the Marmion gneiss, defining the dominant structural fabric.

Two contrasting models have been suggested for the tectonic development of the Finlayson belt. Fold axes were inferred from stratigraphic reversals and the Finlayson belt was interpreted as a sagducted synclinal keel (Stone and Kamineni, 1989; Stone et al., 1992). Alternatively, Stone (2008, 2010) interpreted three fault-bounded allochthonous sub-belts based on the two different measured ages and a third younger age inferred from petrographic similarities to the younger Steep Rock greenstone belt to the south. Due to the lateral heterogeneity of units and lack of marker horizons, lithologic mapping of the Finlayson belt has not resulted in an equivocal structural model. However, a detailed structural and kinematic study of the greenstone belt allows us to test the validity of either hypothesis and explore implications for the regional deformation history of the south-central Wabigoon subprovince. We visited lake-shore exposures throughout the belt and conducted detailed structural mapping (Fig. 1). We have produced a structural framework and metamorphic-deformational history that is wholly based on field data and observations. In this paper we compare this framework to the predictions of the competing tectonic models, and place the local deformational history in regional context.

2. Geological setting

The Superior Province in Canada preserves one of the largest assemblages of Meso- to Neoarchaean terranes. The individual terranes that make up the Superior Province amalgamated progressively from north to south within the 2.72–2.68 Ga tectonism known as the Kenoran orogeny (Polat and Kerrich, 2001; Percival et al., 2006; Percival, 2007a), at which time most workers agree that some form of accretionary tectonics was active. Northward dipping fabrics associated with the east-west trending terrane boundaries have been interpreted as northward directed subduction zones active during the accretion period (Calvert et al., 1995; Whalen et al., 2002; White et al., 2003; Musacchio et al., 2004). The Wabigoon subprovince is bounded to the south by the Quetico terrane metasediments, which separate the TTG-greenstone terranes of the Wabigoon and Wawa subprovinces (Percival, 1989, 2007a; Percival and Williams, 1989). The east-west trending southern margin of the Wabigoon subprovince has been interpreted as a fault with dextral transpression (Williams, 1990; Bauer et al., 1992; Peterson and Zaleski, 1999), known as the Quetico fault (Fig. 1a).

The Marmion TTG gneisses are bounded on three sides by greenstone belts: the 2.9–3.0 Ga Finlayson belt, the 3.0 Ga Lumby Lake and 2.7 Ga Steep Rock greenstone belts (Fig. 1a). The contact relationships between the greenstone belts and the tonalite gneisses are discussed by Thomlinson et al. (2003) and Stone (2010). The younger Steep Rock greenstone belt has a documented unconformity at its base, suggesting that it was deposited onto the exposed Marmion TTGs (Wilks and Nisbet, 1988; Stone, 2010). Mapped contact geometries suggest that the Lumby Lake belt is in fault contact with the Marmion gneiss and several major faults parallel to the boundary have been documented within the belt (Thomlinson et al., 1999). The contact between the Finlayson and the Marmion gneiss is named the Marmion Shear Zone (Fig. 1a), which links to the north with the Red Paint Lake Shear Zone (Davis and Jackson, 1988; Stone, 2008) and is cut to the south by the Quetico fault (Bauer et al., 1992; Stone, 2008). The Marmion Shear Zone has been intruded by Diversion Stock granitoids and the shear zone core is not exposed (Fig. 1b). The western boundary is similarly poorly exposed and separates the Finlayson belt from the Dashwa gneisses in the south and the Hardtack gneisses to the northwest. The dome-shaped Dashwa gneisses have a younger 2.68 Ga intrusive pluton core (the Eye-Dashwa pluton), which along with steep lineations that indicate vertical kinematics of a rising gneiss dome relative to the surrounding greenstone belts (Borowski, 2013) have been suggested to show the strongest evidence for solid state gneiss diapirism in the region (see also Schwerdtner et al., 1979; Schwerdtner, 1982).

The interpretation of a synformal keel Finlayson belt was derived from a coarse-grid gravity study (Gibb et al., 1988) and inferred synclinal fold axes (Stone and Kamineni, 1989) to explain local pillow way-up reversals. A later interpretation by Stone (2008) subdivided the Finlayson belt into three parallel western-, central- (or Witch Bay) and eastern sub-belts, based on two maximum age dates of a 2.931 Ga felsic tuff and a 3.003 Ga quartz-feldspar volcanic porphyry from the greenstone belt's western and eastern zones, respectively. A youngest zircon detrital age from a conglomerate puts the upper limit on sedimentation in the eastern sedimentary unit at 2.997 Ga (Stone, 2010), which falls within the published age range that spans at least 70 million years. The third belt that separates the eastern and western subdivisions is different, with a lighter shade of green in outcrop, although the lithological assemblages (pillow to massive basalt flows and diverse sediments) are similar. The difference was related to contrasting metamorphic grades with amphibolite facies on the margins and greenschist facies in the centre (see Stone, 2010). We test this explanation below, as well as the hypothesis that the petrographic contrasts could represent primary compositional differences across the greenstone belt with associated variations in the extent of low-grade metamorphic overprinting.

3. Field and petrographic observations

The Finlayson belt has undergone multiple deformation events causing the development of tectonic structures including folds, faults and grain-scale mineral fabrics. Below we describe each of these and their spatial variations before developing the structural history of the belt. Due to recent lowering of the water level at Finlayson Lake, fresh exposures are found predominantly along the lake-shore outcrops. Our contribution adds detailed, small-scale structural mapping to the regional mapping by Stone (2008). By distinguishing deformational fabrics of different kinematics, metamorphic grade and relative timing, we are able to investigate the structural evolution in more detail.

In order to test the hypotheses for the geometry of the greenstone belt, we made detailed structural transects across and

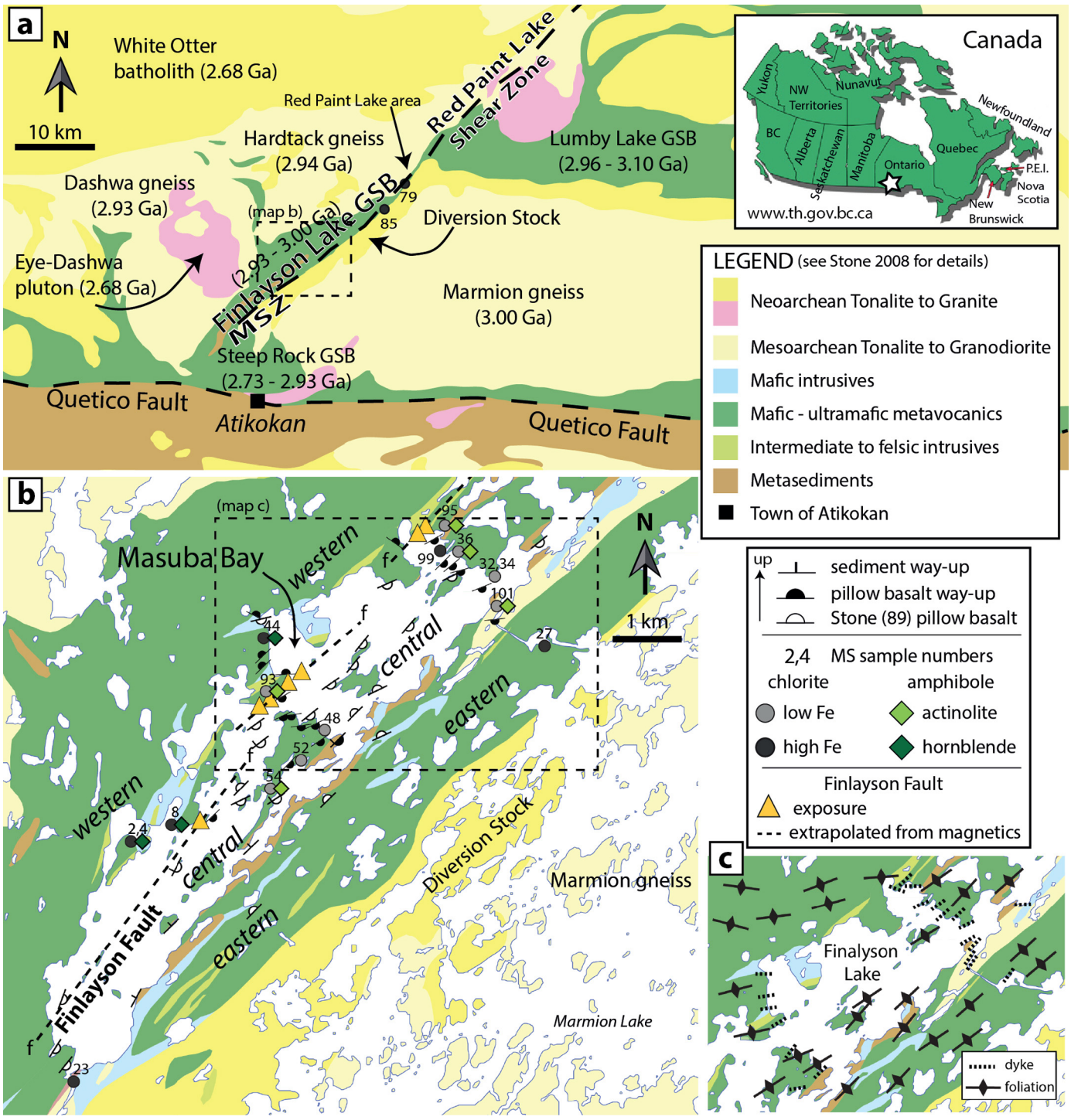

Fig. 1. Maps of the Finlayson Lake greenstone belt adapted from Stone (2008). Location in Ontario shown by white star on the top right map of Canada. (a) Simplified regional map of the Lumby Lake, Finlayson Lake and Steep Rock greenstone belts (GSB) and associated gneiss domes, also showing the Quetico Fault, Marmion Shear Zone (MSZ) and Red Paint Lake Shear Zone. (b) Enlarged map of the Finlayson belt showing: Pillow basalt way-up orientations; low- and high Fe chlorite groups (circles) for selected samples (numbers); hornblende or actinolite amphibole occurrence (diamonds), locations with no diamond symbol have no amphibole preserved; mapped locations of altered fault zone (triangles); and extent of fault beneath Finlayson Lake as extrapolated from magnetic data and field exposures. (c) Dashed area outlined in map (b) showing the strike of sub-vertical foliation and dyke data for that area. White areas (b and c) are lakes.

along strike, focussing on changes in facing direction, faults, folds, and foliations which preserve kinematic information. Field and microstructural studies have revealed evidence for at least 4 deformation episodes affecting the Finlayson belt. The structural fabrics and mineral assemblages formed during each deformation are described below.

3.1. Belt-scale fabric and dykes

Overall the Finlayson belt has a well-defined structural fabric that is easily observed in exposures and aerial photography. The predominant structural fabric and lithological contacts are sub-vertical and strike parallel to the eastern boundary at

approximately 040–060° (Fig. 2a–c). In the west the mean strike is ENE and becomes more clustered with a NE strike in the eastern portion of the belt (Fig. 2a–c), consistent with previous work (Stone, 2008). Dykes are common throughout the Finlayson belt and consist of mostly mafic with few felsic dykes. Felsic dykes are more common in the eastern portion of the belt (see Section 3.6). Predominantly, dykes intrude parallel to the structural fabric (Figs. 1c and 2a). Dykes that are at an angle to the structural fabric are folded. The dyke patterns suggest that magmatism was ongoing before, during and after deformation events of the Finlayson belt.

3.2. Micro-scale inclusion fabric

The oldest fabric has only been observed as mineral inclusions within younger hornblende crystals. Microscopic observations of a coarse gabbroic unit (sample MS008) show the sub-mm scale inclusion fabric set within aligned hornblende (Fig. 2f). The inclusion assemblage consists of plagioclase, quartz and ilmenite that are aligned and parallel across the thin section (Fig. 2f). We interpret the alignment on the inclusion mineral assemblage to represents a prograde metamorphic foliation (S_1), that is no longer preserved on the macro scale. The angle between and lineated hornblende is ~30° with variations of >20° related to the variation of the lineation fabric. The kinematic signature of S_1 is not evident in the collected samples. Although the inclusion fabric has been almost entirely overprinted, this inclusion assemblage allowed us to calculate the prograde metamorphic pressure–temperature conditions (see Section 5).

3.3. Greenstone belt way-up facing orientations

A first-order question for greenstone belt structure is identifying the symmetry across the belt. The sagduction model predicts an overall synclinal symmetry with both outermost limbs facing inward, as was originally proposed for the Finlayson belt by Stone and Kamineni (1989). To test the overall structure of the Finlayson belt we mapped the facing direction for several detailed transects across the belt in as much detail as possible and patterns were detected on multiple scales. Palaeo way-up facing orientations can be interpreted from pillow basalts by identifying the lobate tops and downward pointing tails. Due to the high degree of flattening experienced in the Finlayson belt, many pillow basalt exposures are ambiguous with regards to way-up facing direction. Therefore, we only include unambiguous pillow facing orientations from this study and those mapped by Stone et al. (1992) in Fig. 1b.

3.3.1. Belt-scale pillow reversal

Variations in pillow facing orientations are observed in the Finlayson belt and have previously been reported on geological maps (Stone and Kamineni, 1989). Our detailed transects show two domains of pillow basalt facing orientations. In the western portion of the Finlayson belt, pillows face predominantly northwest, whereas in the central portion of the belt they are southeast facing, such that the two domains face outwards (Fig. 1b). Pillow basalts are only locally preserved in the eastern Finlayson belt (see Sections 3.4 and 3.6). The two domains of pillow facing orientations are separated by a 3–7 m wide linear zone of intense foliation and alteration (see triangles in Fig. 1b). The alteration assemblage is predominantly ankerite and pyrite and the pre-existing rock structure has been overprinted by an intense foliation. The edges of the most intense alteration can be very sharp (<1 m), but typically grade to unaltered rock over a distance of 1–5 m. Although no kinematic indicators were observed around this feature, the linear geometry and concentrated alteration suggests a belt-scale fault separates the two domains of way-up orientations (Fig. 1b). This newly identified fault, here named the Finlayson Fault, may have taken advantage of a pre-existing weakness such as a larger-scale anticline axis, which would be consistent with the belt-scale pillow reversals. The observed fault locations coincide with linear magnetic high features (Ontario Geological Survey, 2009) and in Fig. 1b the fault has been traced along the magnetic anomaly that coincides with the observations. The pillow facing orientations are outward, opposite to the facing directions predicted by synclinal symmetry.

3.3.2. Structures leading to local pillow basalt reversals

Sub-vertical lithological units within each way-up facing domain defined above are mostly conformable on traverses perpendicular to the structural fabric. The strike and dip of the lithological contacts are parallel to the strongest foliation. A planar alignment (S_2) of predominantly plagioclase and weakly aligned hornblende is parallel to the lithological contacts. The weak amphibole lineation (L_2) is observed in coarser gabbroic units (Fig. 2f) and seen in thin section for finer grained lithologies. Amphiboles in rare metagabbros show a mean plunge of 45° to 70° within the S_2 foliation. Co-planarity and definition of these fabrics by alignment of the hornblende motivate us to interpret the weak amphibole lineation as co-genetic with S_2 foliation ($S_2 - L_2$ fabric).

We were not able to identify any repetition of sedimentary or volcanic packages which might support a hypothesis of 100 m-scale folding across the belt. Folds are observed throughout the belt, but these are typically localised and small scale with a wavelength of a few centimetres to 1 m (e.g. Fig. 2h–i). The long limbs of the folds are parallel to the S_2 structural fabric (Fig. 2h–i) and fold axes across the belt are consistently steeply plunging sub-parallel to L_2 (Fig. 3b). Although pillow basalt way-up orientations are mostly consistent in the two domains either side of the Finlayson Fault (Section 3.3.1), reversals have been documented by Stone and Kamineni (1989) and we observed local zones of palaeo way-up reversals. The outcrop in the Masuba Bay area of Finlayson Lake exposes one fold hinge of a larger (20 m wavelength) isoclinal F_2 fold (Fig. 3a). The fold asymmetry records sinistral kinematics and within the short limb of the fold, pillow way-up orientations are reversed. A parasitic 1 m wavelength fold shows the same sinistral sense of rotation and folding of preserved pillow basalts around the axial trace (Fig. 2h).

The intensity of the S_2 structural fabric is generally consistent across the Finlayson belt. A few discreet small shear zones are observed parallel to the S_2 foliation. One example is a sinistral 50 cm wide shear zones striking sub-parallel to the local S_2 foliation in the central portion of the Finlayson belt (Fig. 2j). Fig. 2j shows sheared pillow margins preserving sinistral kinematics. The shear structure preserves the same sinistral kinematics and amphibole mineralogy as the S_2 foliation and we interpret the two structures to be syn-kinematic. In the eastern portion of the Finlayson belt S_2 structures are only observed in the hinge zones of F_2 folds, where the intersection angle of the fold limbs and later overprinting retrograde foliation (see Section 3.4) is increased (Fig. 2i).

3.4. Schistosity

The dominant structural fabric observed throughout the Finlayson belt is a sub-vertical chlorite foliation (S_3), which is penetrative from belt to thin section scale. The chlorite-foliation developed sub-parallel to the S_2 foliation and is defined by retrogressive chlorite replacing amphibole (Fig. 2d). The cross-cutting relationship is locally revealed by overprinting at a moderate angle across the asymmetric F_2 fold hinges (Fig. 2i). No mineral lineation is associated with S_3, but intersection lineations of the sub-parallel S_2 and S_3 fabrics are commonly observed in outcrops and easily mistaken for mineral lineations. The intensity of the foliation is directly proportional to the amount of chlorite growth, which is correlated with the extent of amphibole to chlorite retrogression and is strongest at the eastern boundary (Fig. 2a–e). The most intensely

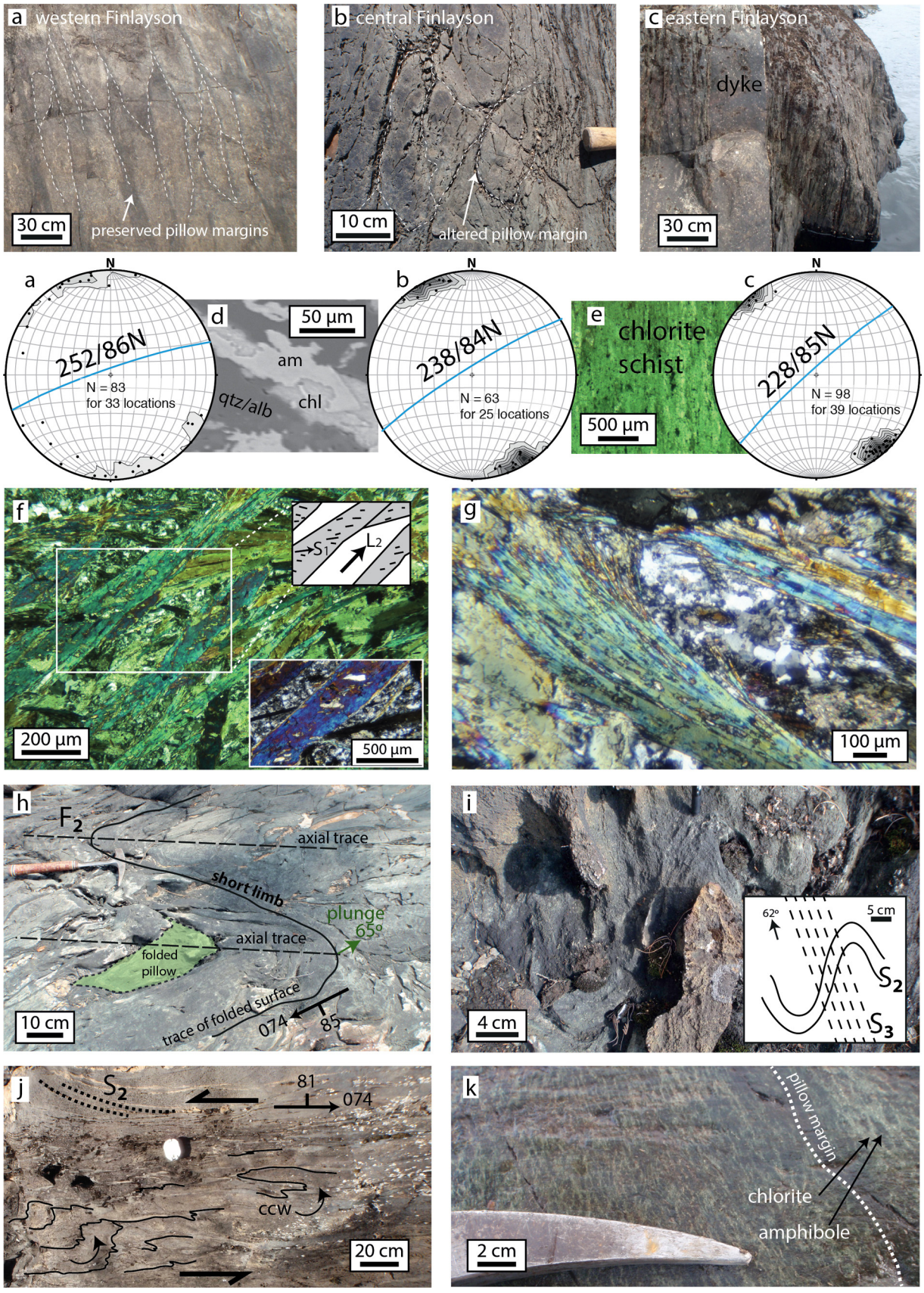

Fig. 2. Field pictures from the Finlayson belt. (a) Pillow basalts in the western Finlayson area showing well-preserved pillow margins. Structural fabrics shows a mean strike and dip of 252/86 N with a 95% confidence of 17° (stereonet). (b) Pillow basalts in the central portion of the Finlayson belt show partially retrogressed pillow margins. Foliation has an average strike and dip of 238/84 N with a 95% confidence of 6° (stereonet). (c) Basalts are retrogressed to strongly foliated chlorite schists in the eastern Finlayson and this photo shows a mafic dyke intruding parallel to the dominant structural fabric. Foliation is tightly clustered around 228/85 N with a 95% confidence of 3° (stereonet). (d) Backscatter image of a basalt in the western Finlayson area showing partial retrogression of amphibole to chlorite. (e) Plane polarised transmitted light thin section image

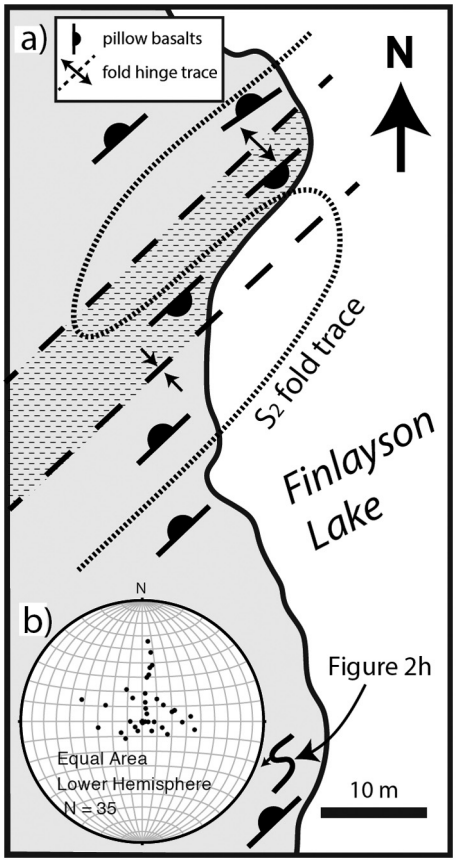

Fig. 3. (a) Field map of pillow reversal zones in short limbs of sinistral F_2 folds from Masuba Bay area (See Fig. 1). Dashed lines show the trace of the fold hinge and dotted line traces out the isoclinal fold. Location of parasitic fold (Fig. 2h) is indicated in lower right corner. (b) F_2 fold axes from across the Finlayson belt showing steep to sub-vertical plunges.

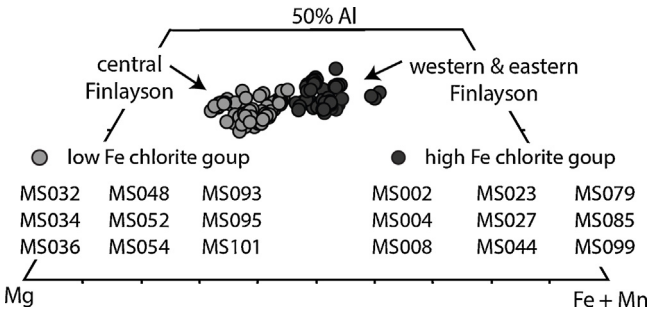

Fig. 4. Plot of chlorite compositions measured by microprobe for 18 samples and 165 chlorite analyses. Locations of samples are shown in Figure 1b. Samples MS079 and MS085 are part of the eastern Finlayson farther north at Red Paint Lake (Fig. 1a). Samples are grouped spatially into eastern-western Finlayson (dark circles) and central Finlayson (light circles) as determined from field descriptions of dark or light green basaltic units. Chlorite compositions from western and eastern Finlayson samples show a complete overlap in composition (dark circles). The spatial groupings show a clear separation into higher- (dark circles) and lower- (light circles) iron compositions.

foliated units are chlorite schists, where the phyllosilicates form pervasive parallel foliation surfaces and completely overprint the $S_2 - L_2$ structures (Fig. 2c and e). These chlorite schists are found within 1–2 km of the eastern margin of the Finlayson belt striking sub-parallel to the eastern boundary at 230° with a sub-vertical dip (Fig. 2c). To the west the foliation is weaker, displaying stronger chlorite foliation in fine grained rocks such as pillow margins and weaker overprint in coarse grained rocks. In areas of the weakest foliation, chlorite retrogression only partially replaces amphiboles as shown in Fig. 2d. Parallel phyllosilicates and flattened clast symmetry of quartz grains are consistent with pure shear strain within the quartz ductile regime during retrogression.

3.5. Mineralogy

Stone (2010) mapped different structural units in the Finlayson belt based on darker green metabasalts in the western and eastern portions and lighter green metabasalts in the central portion (Fig. 1b). Stone (2010) attributed these to different metamorphic grades of dark hornblende (amphibolite grade) versus light actinolite (greenschist grade) and used this distinction to correlate parts of the Finlayson to other nearby greenstone belts. Here we relate the paragenesis to the observed structural fabrics described above and combine these observations with electron microprobe mineral analyses in samples from across the belt in order to test the origin of the colour differences.

Sample MS008 (Fig. 2f) from the western portion of Finlayson belt (Fig. 1b) was selected to represent the best preserved higher grade metamorphic assemblages with only weak retrogression seen as acicular amphiboles (Fig. 2g). This sample revealed a mineral assemblage preserved as inclusions (Section 3.2; Fig. 2f). The inclusion mineral assemblage consists of hornblende, plagioclase, quartz and ilmenite ± epidote. This inclusion assemblage forms with a preferred orientation (S_1) and records a prograde foliation preserved within the $S_2 - L_2$ fabric.

The peak metamorphic paragenesis is variable in units depending on their bulk composition. The assemblages consist of amphibole + plagioclase + ilmenite, amphibole + plagioclase + ilmenite + quartz and amphibole + plagioclase + epidote + ilmenite ± quartz. The least retrogressed units that best preserve the $S_2 - L_2$ fabric are typically gabbroic with weakly lineated amphiboles (L_2). Sample MS008 preserves a peak paragenesis of amphibole + plagioclase + ilmenite, which was used for pressure–temperature and pseudosection calculations (see Section 5).

The retrogressive overprinting assemblage, which increases in abundance from west to east includes chlorite, actinolite, albite, quartz, titanite and epidote. The intensity of retrogression varies considerably from weakly altered units with preserved hornblende to intermediate retrogression including partial replacement of hornblende by actinolite and finally to chlorite schists with no preserved amphiboles. The majority of chlorite retrogression is accompanied with the development of the foliation. Poikilitic and euhedral titanite is common around relict ilmenite grains throughout the Finlayson belt and overgrows both the L_2 fabric of the amphiboles and S_3 chlorite foliation.

We compared the amphibole compositions across the belt in order to test the contrasting metamorphic grades that Stone (2010) proposed. Actinolite is found in the central Finlayson belt and rare remnant actinolite is preserved in the eastern portion of the Finlayson belt (Fig. 1b). Hornblende is only preserved in the western portion of the belt (Fig. 1b). Therefore, the distribution of actinolite versus hornblende as suggested by Stone (2010) does not explain

of chlorite schist. (f) Two examples from single thin section of coarse gained metagabbro (sample MS008) with coarse lineated hornblende (grey shaded L_2) with aligned inclusions (S_1) within hornblende. (g) Acicular amphibole growth of L_2 hornblende in sample MS008. (h) Sinistral F_2 fold in the Masuba Bay area, showing folded pillow basalts. (i) Cryptic F_2 fold in the central Finlayson visible in hinge zones. (j) Sheared pillow basalts in a sinistral shear zone. Deformed pillow margins (solid lines) and S_2 foliation sheared into parallelism with high strain zone (dotted lines) show sinistral kinematics. (k) Coarse grained pillow basalts.

the occurrence of a colour difference by metamorphic grade within the Finlayson belt. We analysed chlorite ($n = 164$) and found that chlorite compositions from the lighter and darker metabasalts, as mapped by Stone (2010), correspond to a clear division of lower-iron and higher-iron compositions (Fig. 4). The chlorite in the darker green volcanics corresponds to the high-iron group and have a strong pleochroism and deeper green colour. The data shows that the lighter green colour of the basalts in the central Finlayson volcanics (previously named the Witch Bay sub-belt, see Stone (2010)) is coincident with a paler green chlorite with lower iron content (Fig. 1b).

The origin of this chemical difference in the chlorite may reflect different parental sources with primary differences in magnesium-iron ratios. Our limited whole rock geochemistry dataset suggest that the lighter basalts have higher magnesium-iron ratios ($n = 2$) than the darker basalts ($n = 5$), consistent with the differences observed in the chlorites. However, the current whole-rock geochemistry dataset is not extensive enough to exclude any other origins for the colour differences, such as preferential sequestering of Fe by other phases, such as pyrite, and the extent of retrogression.

3.6. Coarse-grained pillow basalts

Most earlier structures have been overprinted in the eastern portion of the Finlayson belt (see Section 3.4). The only preserved lithological structures are pillow basalts that have an unusual coarse grained texture (Fig. 2k) with the primary S_2 fabric preserved. Coarse grained pillow basalts are found as discrete zones located immediately adjacent to competent felsic intrusive dykes within the region of intensely foliated chlorite schists. The typically dominant foliation in this region is very weak to absent in the preserved pillow basalts. These pillows have similar aspect ratios to the those in the western portion of the Finlayson belt and were likely also deformed under the same conditions (see Section 3.3.2). However, a coarse grained metamorphic mineral texture is unique to the eastern pillow basalts (Fig. 2k). The mineralogy consists mainly of coarse euhedral amphiboles with no preferred orientation. The margins of the amphiboles are retrogressed to chlorite, but no penetrative foliation is developed. The proximity to intrusive dykes suggest that the coarse grained texture may be resultant from contact metamorphism during intrusion of the felsic dykes. This coarse texture is not found beyond 10–15 m from the intrusive dykes.

3.7. Veins

Veins in the Finlayson belt of multiple generations include monomineralic and polymineralic combinations of quartz, calcite and/or ankerite ± pyrite, chalcopyrite and accessory monazite. The veins are emplaced predominantly vertically along pre-existing structures and have mutually crosscutting relations between the different populations of veins. Quartz veins are the most common and are boudinaged and folded (Fig. 5). Boudinaged quartz veins show pure shear kinematics with stretching in both dip- and strike-parallel axes, parallel to foliation. Deformed quartz veins within the zones of coarse grained pillow basalts (see Section 3.6), are emplaced crosscutting the S_2 fabric. The quartz veins are folded and boudinaged axial planar to the S_3 foliation (Fig. 5). The felsic dykes that are spatially associated with the coarse pillow basalts show the same generation of folded veins within them (Fig. 5b). These veins are recording a shortening that postdates the S_2 fabric. The amount of shortening measured in three quartz veins that postdate S_2 and show only S_3 shortening increases from west to east. Shortening was calculated by measuring the original length (l_0) of the vein and the final folded length (l_1) (see Fig. 5b for example). The ratio of final to original quartz vein lengths are 15:41 (63%) at the eastern boundary, 31:67 (54%) at approximately 1 km west of the boundary and 268:541 (50%) for veins 2 km west of the eastern boundary. The trend of increasing shortening towards the east is consistent with the intensity of the chlorite retrogression.

Non-planar and discontinuous ankerite veins are concentrated in zones of intense foliation and can range in thickness from sub-cm to massive 1–3 m wide zones of intense veining and alteration. These veins pinch and swell and are associated with massive sulphides that are scattered throughout the Finlayson belt. Massive ankerite zones entrain abundant foliated volcanic wall rock, suggesting that the fluids used the foliation as a conduit, as seen at the Finlayson Fault. Abundant euhedral coarse pyrite grains grow on the mafic volcanic rafts within the ankerite veins. Calcite veins are the most rarely observed vein-type. Most commonly, the calcite veins form as late sub-horizontal veins in the chlorite schists of the eastern margins of the Finlayson belt. The late calcite veins cut the foliation surfaces as well as pre-existing quartz and/or ankerite veins (Fig. 6a). Foliation-parallel calcite veins are also observed, but most commonly in association with quartz as a co-mineralising phase.

3.8. Faults and fractures

The youngest structures in the Finlayson belt are faults and fractures, which show brittle deformation of quartz. These faults are most abundant in the eastern portion of the Finlayson belt. Most faults only accommodate small-scale offset ranging between 5 cm and 5 m. Slip is localised on earlier planar structures (S_2 and S_3) and displacement is measured from offset dykes and veins. Slickensides are observed on exposed foliation surfaces of the chlorite schists of the eastern Finlayson belt (Fig. 6a). Slicks are typically sub vertical and in one outcrop can range in rake between 90° and 70° (Fig. 6a). Fig. 6a shows the relationship of veins, including quartz-ankerite and ankerite veins parallel to the chlorite foliation and sub-horizontal calcite veins cutting the foliation and other vein sets. The calcite veins post-date the S_3 chlorite foliation development (see Section 3.7). These calcite veins are displaced along S_3 foliation surfaces that accommodated slip (Fig. 6b), showing that the S_3 foliation surfaces were reactivated as (small-scale) slip surfaces.

The predominant sense of strike slip recorded along faults is sinistral with only few dextral faults (Fig. 6c). The amount of vertical slip on these faults is not constrained, but if these faults are coeval to the sub vertical slickensides seen on chlorite foliation, we can assume vertical slip is larger than strike-parallel slip. The conjugate orientations of dextral versus sinistral faults are symmetrical around the pole to the chlorite foliation (Fig. 6c). Domains of sinistral faults strike between 350° and 050°, whereas dextral faults strike between 230° and 320°, separated across the orientation of S_3 foliation (Fig. 6c).

3.9. Boundaries of the Finlayson belt

Greenstone belt boundaries are key to unravelling the kinematic history of greenstone-TTG contacts and the tectonic setting that juxtaposed supracrustal with crustal terranes. The ambiguity of the contacts as either large shear zones, slightly faulted non-conformities or both is often difficult to establish in any Archaean greenstone-TTG terrane. Here we present the observed constraints focussed on the eastern boundary of the Finlayson belt. The western boundary to the Dashwa (Fig. 1a) was investigated as part of an unpublished study (Borowski, 2013) and we present evidence for boundary kinematics from his field work and other published studies for completion. The northwestern contact to the Hardtack TTGs was observed at one small exposure in the Red Paint Lake area (Fig. 1a).

3.9.1. The eastern boundary

The eastern boundary of the Finlayson belt has been interpreted as the Marmion Shear Zone or Marmion Fault, which marks the southwestern extension of the Red Paint Lake Shear Zone (Fig. 1a). The Marmion Shear Zone is not exposed and the structure has been intruded by the Diversion Stock granitoids (Fig. 1b), preventing any direct field observations and kinematic interpretations. The only available minimum age constraint for movement along the

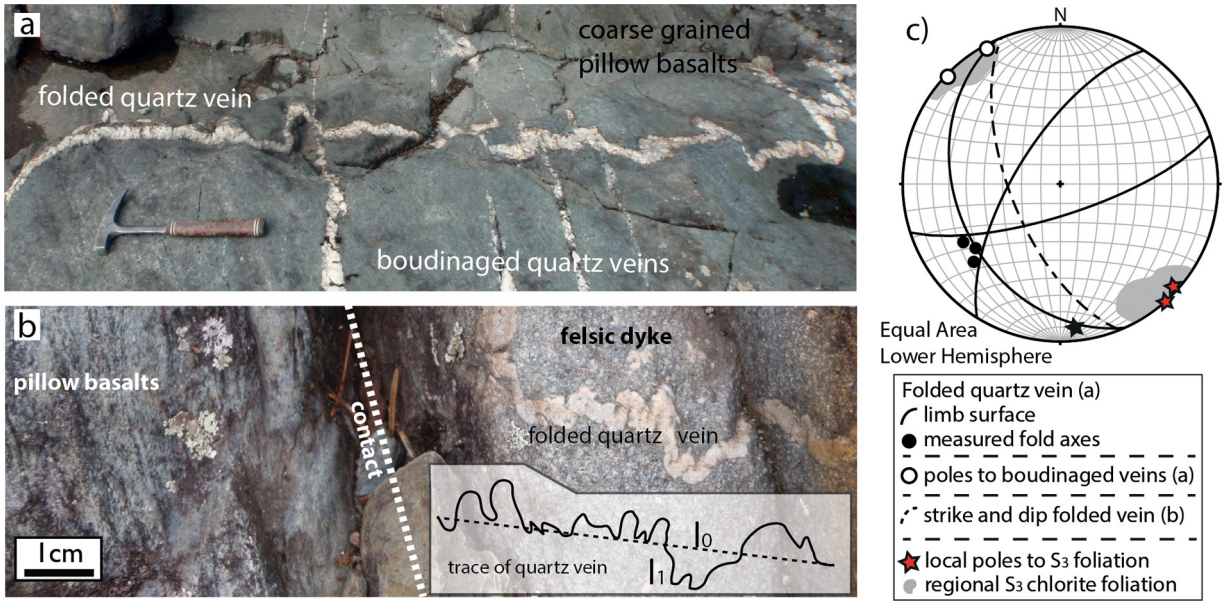

Fig. 5. Deformed quartz veins in the Finlayson belt. (a) Folded and boudinaged quart veins within coarse-grained pillow basalts. (b) Intrusive felsic dyke with folded quartz vein recording shortening. Dashed black line (l_0) shows trace of original length and solid line (l_1) is the trace of the final folded vein. (c) Orientation data for limbs of folded quartz veins (lines) and poles to boudinaged veins (open circles). Regional (shaded area) and local (red star) chlorite foliation is plotted for comparison. (For interpretationof the references to colour in this figure legend, the reader is referred to the web version of this article.)

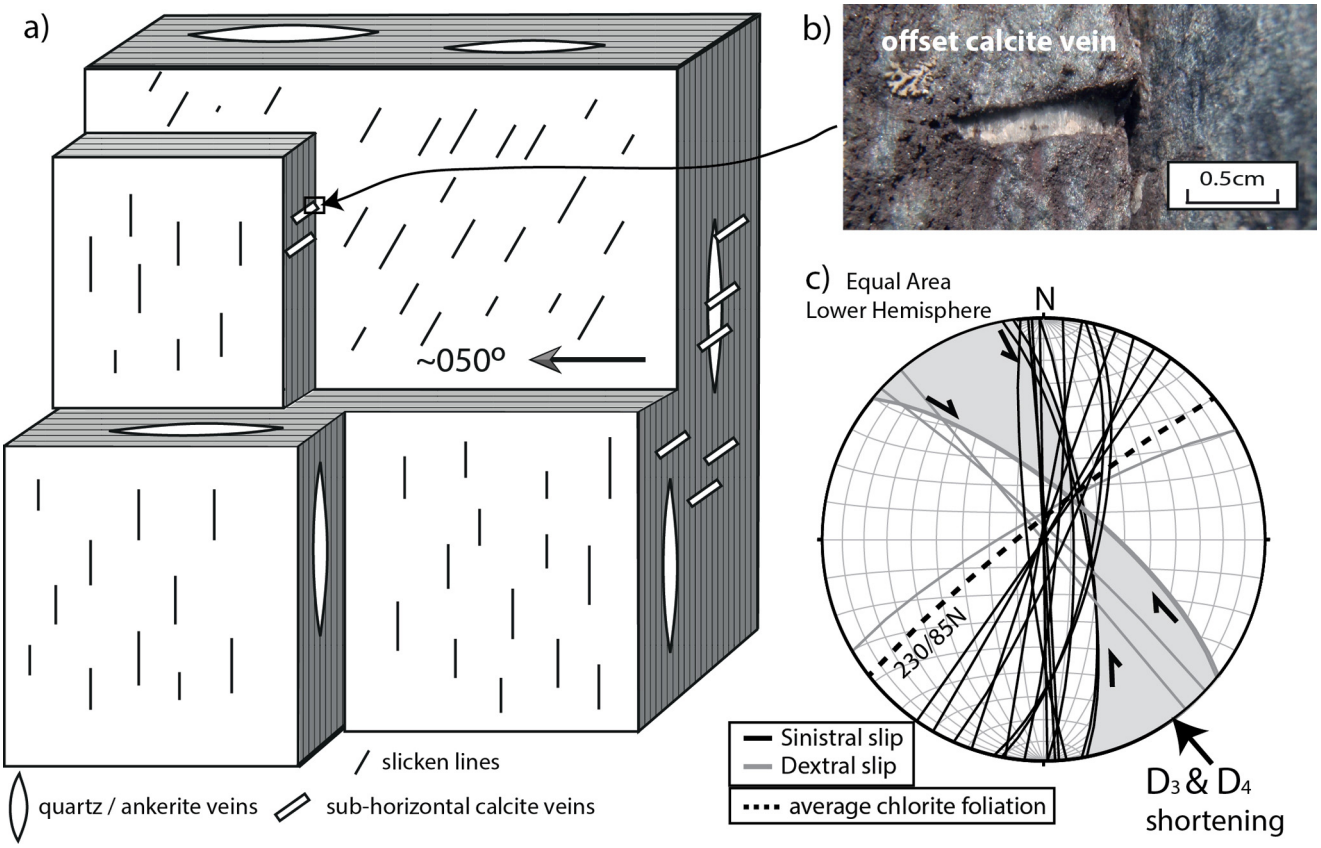

Fig. 6. (a) Block-sketch of intensely foliated chlorite schists in eastern Finlayson. Exposed foliation surfaces (not to scale) show slickensides with oblique to vertical slip. (b) Sub-horizontal calcite vein showing offset along foliation plane. (c) Sinistral (black lines) and dextral (grey lines) brittle faults from the Finlayson belt. The grey shaded area represents a conjugate set of sinistral and dextral faults at the same outcrop and show the compression field. Dashed line is the average chlorite foliation (230/50 N – strike/dip), which separates the orientations of dextral and sinistral structures, suggesting sub-parallel shortening axes for D_3 and D_4.

Marmion Shear Zone is from the approximately 2.7 Ga Quetico Fault that cuts it to the south (Fig. 1a). Metasediments close to the eastern margin of the Finlayson belt may include abundant mm-sized feldspar grains and carry rare tonalite blocks up to 20 cm large suggesting that the greenstone belt units were deposited onto or close to exposed felsic basement. The presence of exposed felsic basement is consistent with Marmion-age 3.0 Ga inherited zircons in the conformable sedimentary units of the Finlayson belt (see Stone, 2008), further suggesting that exposed felsic terranes similar in age and composition to the Marmion gneisses were eroded into the basin before the greenstone belt was deformed. Although the age of Diversion stock is poorly constrained, the structural relations demonstrate that it intruded along the already established contact between the Finlayson belt and Marmion TTGs. From published maps (Stone, 2008) the boundary between the Finlayson belt and Diversion stock is expected to be exposed along shoreline outcrops in the Marmion Lake and Red Paint Lake to the east and north of Finlayson Lake, respectively. At each expected boundary location a preferentially eroded 30–50 m wide zone was observed, separating Finlayson mafic volcanics (chlorite schists) from Diversion Stock granitoids. One location showed remnant slivers of the Diversion Stock granitoid in contact with the greenstone belt. From this location we were able to measure the strike and dip of the eastern boundary. On average the contact strikes 050° (035–070°) and dips 75° (60–80°) to the southeast. The boundary zone is characterised by well foliated mafic volcanics and a series of granitoid dykes that increase in density towards the main Diversion Stock intrusion over approximately 50–100 m. The granitoid dykes are parallel to the boundary and greenstone belt fabric and are petrographically identical to the main Diversion Stock intrusion. Although some dykes are undeformed, many have been fractured, suggesting localised brittle deformation postdating their intrusion.

3.9.2. The western boundary

In the west the Finlayson belt is bounded by two different TTG terranes, the 2.93 Ga Dashwa gneiss and the 2.94 Ga Hardtack gneiss. Both are younger than the 3.0 Ga Marmion TTGs and the Finlayson belt. The Dashwa TTGs, amongst other Wabigoon subprovince gneiss domes, have been cited amongst the key examples of solid state gneiss diapirism within the Superior Province (Schwerdtner et al., 1979; Schwerdtner, 1984, and unpublished fieldwork: Borowski (2013)). They document concentric foliation patterns, the younger 2.68 Ga Eye-Dashwa intrusive core, steeply plunging ductile lineation structures and greenstone belt-down kinematics supporting diapiric tectonic processes. Schwerdtner (1990) refuted the diapiric model based on structural tests of relative timing of folding and doming, suggesting that upright folding in the TTGs occurred prior to the doming phase. We observed better-preserved ductile deformation close to the western margins of the Finlayson belt, consistent with our observations of decreasing retrogression from east to west.

The northwestern contact of the Finlayson belt to the Hardtack gneisses has only been documented in published maps (Stone and Kamineni, 1989; Stone, 2008). We observed the contact to the Hardtack gneiss at Red Paint Lake (Fig. 1a), where the northern extent of the Finlayson Lake greenstone belt is exposed. The contact is faulted and the Hardtack tonalites brecciated. The amount of offset, kinematics or preexisting structures was not identified from this limited exposure. We were not able to investigate this contact any further.

4. Strain interpretations

The Finlayson Lake greenstone belt shows consistent kinematic indicators across the entire belt with early ductile fabrics, retrogressive overprint and late stage minor brittle faulting. In this section we discuss and compare the strain that resulted in the various structures described above in order to constrain the deformational history of the greenstone belt.

4.1. Sinistral transpression at amphibolite facies

The prograde foliation (S_1), which is preserved as inclusions within lineated hornblende (L_2), has been almost entirely overprinted and cannot be conclusively oriented. However, S_1 records an early deformation with the fabric formed at an angle of ~30° to L_2 (Fig. 2f). The S_2 deformation occurred at amphibolite facies as seen from preserved hornblende lineations in the western portion of the Finlayson belt. Structures include sinistral folds with steep fold axes parallel to L_2 and local sinistral shear zones (Section 3.3.2). Both types of structures are kinematically consistent with sinistral transpression during formation of $S_2 - L_2$. All these fabrics can be explained by a horizontal north-south shortening.

4.2. Pure shear at greenschist facies

The S_3 retrogressive chlorite foliation clearly cross-cuts and overprints the $S_2 - L_2$ fabric (Section 3.4). There is no textural evidence for simple shear during the development of S_3 and all outcrops display fabrics showing flattening during chlorite retrogression. The well developed chlorite foliation of the eastern Finlayson suggests a southeast-northwest trending horizontal shortening axis, perpendicular to the eastern boundary (Figs. 2c and 6c). The orientation of the greenschist facies shortening axis can be contrasted to the shortening axis interpreted from the older amphibolite facies structures and records a 40° to 50° change in the shortening direction. The amount of shortening measured in three quartz veins that post-date S_2 and show only S_3 shortening decreases away from the boundary from 63% at the boundary, to 54% at 1 km and 50% at 2 km away perpendicular to boundary. Our observations demonstrate that the Finlayson belt has at least two different sub-parallel fabrics from separate deformation events.

4.3. Brittle reactivation

Late-stage small brittle faults in the eastern portion of the Finlayson belt show slip on pre-existing S_2 and S_3 fabrics. The orientations of sinistral and dextral faults are subdivided (Fig. 6) and define a southeast-northwest compression parallel to the shortening direction interpreted for S_3. Therefore, we infer that shortening continued in the same orientation through the transition from ductile to brittle deformation.

5. Metamorphic constraints

Field and petrographic observations show that the western portion of the Finlayson belt preserves the highest metamorphic grades of the older deformation event. Metamorphic assemblages indicate that peak metamorphism took place at amphibolite-facies conditions, and was followed by progressive retrogression to lower-greenschist-facies conditions. The dominant peak assemblages are amphibole + plagioclase + ilmenite, amphibole + plagioclase + ilmenite + quartz and amphibole + plagioclase + epidote + ilmenite ± quartz, depending on bulk rock composition. Garnet has not been observed anywhere in the belt. The L_2 mineral lineations (Fig. 2f) of peak-metamorphic amphibole are consistent with the sinistral transpression, and position this deformation event at peak metamorphism.

The peak metamorphic minerals, and amphibole in particular, contain a characteristic inclusion assemblage consisting of amphibole + plagioclase + quartz + ilmenite + epidote ± calcite. Plagioclase inclusions (S_1) have a consistently lower X_{An} compared to peak

Table 1
Average hornblende and plagioclase mineral composition used in geothermobarometry. Minerals analysed from Sample MS008. Inclusion compositions measured for D_1 pressure–temperature and matrix compositions measured for D_2.

	Inclusion (D_1)		Matrix (D_2)	
	Amphibole	Plagioclase	Amphibole	Plagioclase
SiO_2	45.25	61.87	44.49	60.84
TiO_2	0.27	n.d.	0.30	0.01
Al_2O_3	10.72	23.91	12.67	24.37
FeO	17.44	0.36	17.05	0.26
MgO	9.85	0.00	9.26	0.00
MnO	0.29	n.d.	0.25	0.01
CaO	11.45	5.14	11.86	5.82
Na_2O	1.34	8.56	1.22	8.16
K_2O	0.28	0.11	0.35	0.11
Total	96.88	99.95	97.46	99.58
X_{Ab}	–	0.72	–	0.75
X_{An}	–	0.28	–	0.25
T (°C)	600 ± 45			625 ± 25
P (MPa)	820 ± 40			635 ± 135

metamorphic (S_2) matrix plagioclase, and amphibole is higher in Al and Ca, and lower in Mg, Fe and Na (Table 1).

Retrogression is progressive, with initial replacement and overgrowth of peak-amphibole by a new, acicular amphibole generation (Fig. 2g). Epidote and quartz (re-)appear in samples where they did not form part of the peak metamorphic assemblage. More intensely retrogressed samples are dominated by chlorite + albite ± actinolite, and may contain carbonate. The retrograde path is accompanied by pure shear kinematics to form the chlorite-defined S_3 foliation. Euhedral titanite growth records a final, static equilibration after the formation of S_3.

The best-preserved amphibolite facies metamorphic assemblages are from the coarse gabbroic unit. In order to further constrain metamorphic conditions, a pseudosection was calculated for the bulk-rock composition of sample MS008 from this unit, using the PerpleX suite of programs (Connolly, 2005). We use the 2002 version of the Holland and Powell (1998) thermodynamic database for mineral end-members, and solid solution models from Holland and Powell (1996, clinopyroxene), Holland and Powell (1998, epidote), Holland et al. (1998, chlorite), Newton et al. (1981, plagioclase), Diener et al. (2007) and Diener and Powell (2012, amphibole), White et al. (2000, ilmenite) and White et al. (2007, garnet) as implemented and modified in PerpleX 6.6.8. Calculations were run at water-saturated conditions and with the oxygen fugacity buffered at Ni-NiO. The resulting diagram is shown in Fig. 7.

For sample MS008, the peak paragenesis is plagioclase + amphibole + ilmenite, and it contains an inclusion paragenesis of plagioclase + amphibole + ilmenite + quartz ± epidote. Combining the pseudosection P–T fields with thermobarometry (Holland and Blundy, 1994) on coexisting plagioclase-amphibole pairs in these two assemblages, suggests conditions of close to 600 °C, 820 MPa for the prograde inclusions, and 625 °C and 635 MPa for the peak conditions (Fig. 7, error bars are the spread in P and T for the various pairs analysed). The peak and inclusion assemblages are used to constrain the P–T range within the respective fields in Fig. 7. Retrograde conditions are bound by the reappearance of chlorite, which is at approximately 550 °C for this bulk-rock composition. For sample MS008 static titanite re-enters the mineral assemblage at temperatures of ~500 °C. Based on our calculations the reappearance of quartz will vary significantly depending on the bulk compositions, with either quartz preceding or postdating titanite retrogression, therefore sample MS008 is used as a guideline only for retrograde conditions.

6. Deformation history of the Finlayson belt

A summary sketch of the Finlayson belt along with its deformation history is shown in Fig. 8. The earliest deformation event (D_1) is only recorded as aligned mineral inclusions and is not seen at the macroscopic scale. From mineral analyses of these inclusions we are able to constrain the pressure and temperature conditions during D_1 at 600 ± 45 °C and 820 ± 40 MPa (Fig. 7), which corresponds to a depth of approximately 27–30 km for typical greenstone belt densities of 2.7–3.0 g/cm^3 (Peschler et al., 2004). The kinematics associated with D_1 are unknown.

The pressure and temperature conditions of D_2 sinistral transpression are coeval with peak metamorphism along a clockwise P–T path at 625 ± 25 °C and 635 ± 125 MPa (Fig. 7), which corresponds to approximately 21–23 km depth. This implies that the Finlayson belt was exhumed by 4–9 km between D_1 and D_2 under near isothermal conditions. Sinistral transpression is recorded on both sides of the Finlayson Fault, which separates the outward facing pillow basalt domains (Fig. 8). Therefore, any major motion on the Finlayson Fault either predates or is synchronous with D_2. Although no kinematics are observed with the Finlayson Fault due to overprinting retrogression, it can be postulated that sinistral strike slip offset was prevalent, if the fault was active during D_2 sinistral transpression. The Finlayson Fault may represent the trace of the anticlinal fold axis that defines the belt-scale pillow facing geometry. There are no constraints to quantify significant fault offset or just preferred flattening of the fold axis along the lineament, but the localised retrogression and alteration of the structure suggests a preferred fluid conduit and our interpretation as a major fault (Fig. 8a).

Magmatic activity was ongoing after sinistral transpression, evidenced by the intrusion of dykes along S_2 foliation (Fig. 1c). Some dykes show weak S_3 chlorite foliation and pure shear, plastically deformed quartz veins supporting the intrusion of dykes before S_3 flattening. Recrystallisation to the coarser texture of pillows related to contact metamorphism strengthens the rock, protecting it against pervasive S_3 chlorite retrogression and shortening. Retrogressive chlorite in these pillow basalts is confined to the margins of amphibole grains (Fig. 2k), also consistent with contact metamorphism occurring prior to the onset of greenschist facies retrogression.

Pure shear, greenschist facies deformation (D_3) is defined by the onset of chlorite retrogression and the development of S_3 foliation with no lineation. Chlorite becomes stable below approximately 550 °C (Fig. 7), which marks the upper temperature limit for the onset of D_3 deformation. Titanite appears at approximately 500 °C (Fig. 7). As ilmenite is still stable during D_3 flattening, the static overgrowth of titanite defines the lower bound for shortening associated with D_3. The pressure conditions for D_3 are unconstrained. The shortening axis rotated from approximately north-south during D_2 to northwest-southeast during D_3, perpendicular to the current orientation of the eastern boundary and the inferred Marmion Shear Zone. The flattening intensifies towards the Marmion Shear Zone from 50% to 63%. The strain estimate of 63% was measured in the contact metamorphic aureoles where strain is at a local minimum. Therefore, we infer that shortening in the chlorite schists was greater than 63% during D_3. The increased intensity of retrogression in the eastern Finlayson may be related to increased fluid flow closer to the eastern margin along the Marmion Shear Zone. Therefore the eastern boundary of the Finlayson belt is likely a crustal scale structure with enhanced greenschist facies retrogression in its proximity.

We have shown that coaxial shortening occurs across the transition from greenschist facies ductile flattening (D_3) into brittle faulting (D_4), presumably during exhumation (Fig. 7). The localisation of brittle deformation in the eastern part of the belt near the

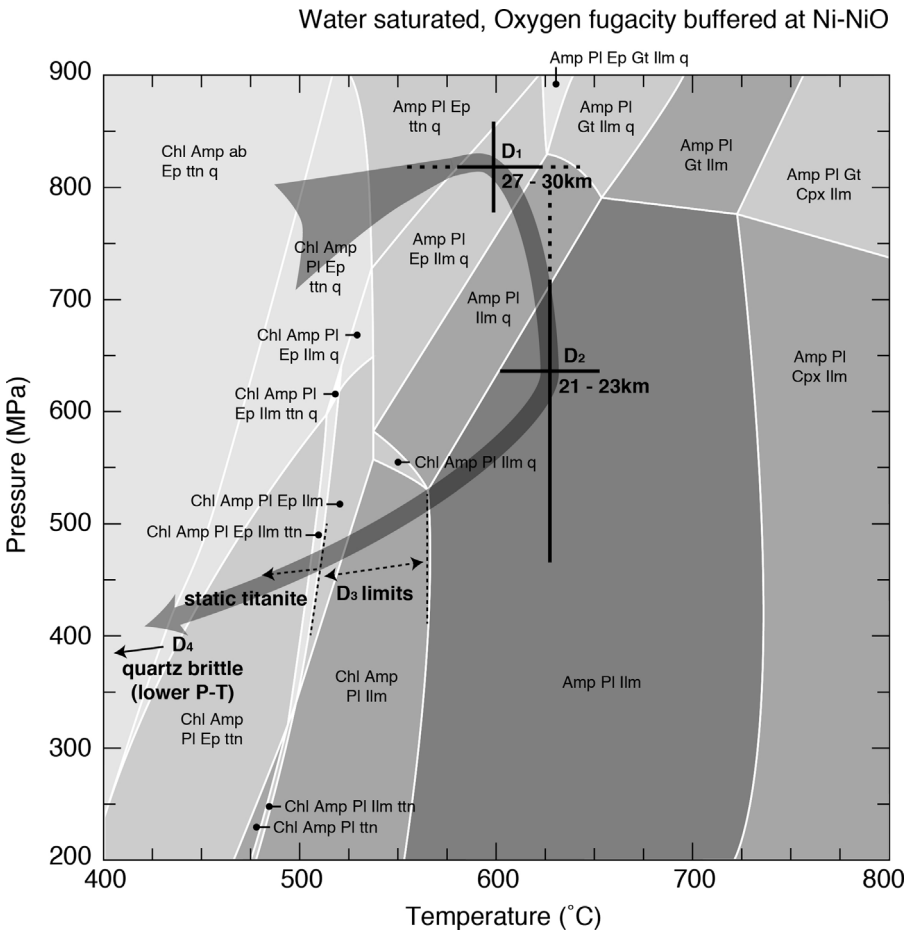

Fig. 7. Pressure–temperature pseudosection calculated for gabbro-sample MS008. Mineral abbreviations follow Kretz (1983) with solid solutions indicated with a capital letter. Prograde conditions (D_1) are constrained by the inclusion paragenesis pl + amp + ep + ilm + q and pl-amp geothermobarometry to 820 ± 40 MPa and 600 ± 45 °C, whereas the D_2 peak metamorphic paragenesis of pl + amp + ilm formed at 635 ± 165 MPa and 625 ± 25 °C. The retrograde paragenesis contains ep, tit and q, and is not well constrained and depends on the bulk composition of the rock. However, we can show that D_3 deformation is constrained by the appearance of retrogressive chlorite (syn-D_3) and the (re-)appearance of static titanite (post-D_3) within quartz-ductile P–T conditions (see arrows showing D_3 limits). The late stage deformation (D_4) occurred within quartz brittle P–T conditions, which plots to lower pressure–temperature conditions, likely at < 400 MPa (~15 km) and < 350 °C.

Marmion Shear Zone supports the hypothesis of continued activity on this structure during exhumation.

The exact ages of deformation events in the Finlayson belt are not known, but can be broadly tied into the tectonic evolution of the Superior Province. The early deformation events (D_1 and D_2) of the Finlayson belt are likely associated with the stabilisation of the 2.9–3.0 Ga Marmion terrane of the south-central Wabigoon subprovince. The larger Wabigoon subprovince is suggested to have formed by accretion of the Marmion, Winnipeg River, eastern- and western Wabigoon terranes as early as 2.92 Ga (see Tomlinson et al., 2004; Percival, 2007a), which is consistent with the youngest ages of the Finlayson belt and adjacent gneiss terranes. A possible cause of the post-D_2 deformation could be related to the accretion of the Wawa, Wabigoon and Quetico subprovinces (Percival and Williams, 1989; Williams, 1990). Amalgamation of Archaean subprovinces to form the Superior Province occurred between 2.72 and 2.68 Ga and has been suggested as a significant part of continental growth during Earth history (Polat and Kerrich, 2001). Brittle reactivation of structures in other greenstone belts in the Wawa subprovince have been tied to the activity of the Quetico Fault at around 2.7 Ga (Peterson and Zaleski, 1999), which lies just to the south of the Finlayson belt (Fig. 1a). Our interpreted NW-SE shortening direction for D_3 and D_4 deformation associated with the reactivation of the Marmion Shear Zone is kinematically consistent with dextral transpression on the Quetico Fault.

7. Resolving the tectonic settings for greenstone belts

The overall dome-and-keel geometry of TTG-greenstone belt provinces is common throughout Archaean cratons, yet the tectonic processes and kinematics that formed them are still much debated. Marshak and Alkmim (2012) compared dome-and-keel provinces globally and subdivided them into three kinematically different settings that allow for orogenic collapse-, accretionary- and diapiric-style tectonics. The subsurface geometry of the inter-dome greenstone belts have been interpreted by seismic and gravity surveys and vary from basin-shaped synclinal belts (e.g. Gibb et al., 1988; Peschler et al., 2004; Ranganai, 2012) to flat sheet-like geometries related to thrust faulting of allochthonous belts (Stettler et al., 1988, 1997; de Wit, 1991). Ground-truthing of the model for synformal greenstone belt structures is drawn from symmetric metamorphic grades and synformal symmetry of mapped units, such as inward facing palaeo way-up orientations of pillow basalts (e.g. Collins and Teyssier, 1990; Minnett and Anhaeusser, 1992; Lin, 2005). On the one hand, field evidence for synformal greenstone belt geometries have been reported in most Archaean terranes, such as the Warrawoona greenstone belt, Pilbara (Collins and Teyssier, 1990) and the Barberton greenstone belt, Kaapvaal (Anhaeusser, 1984). On the other hand, evidence for non-synformal geometries from asymmetric metamorphic grades and structures of the same greenstone belts is also reported (de Wit,

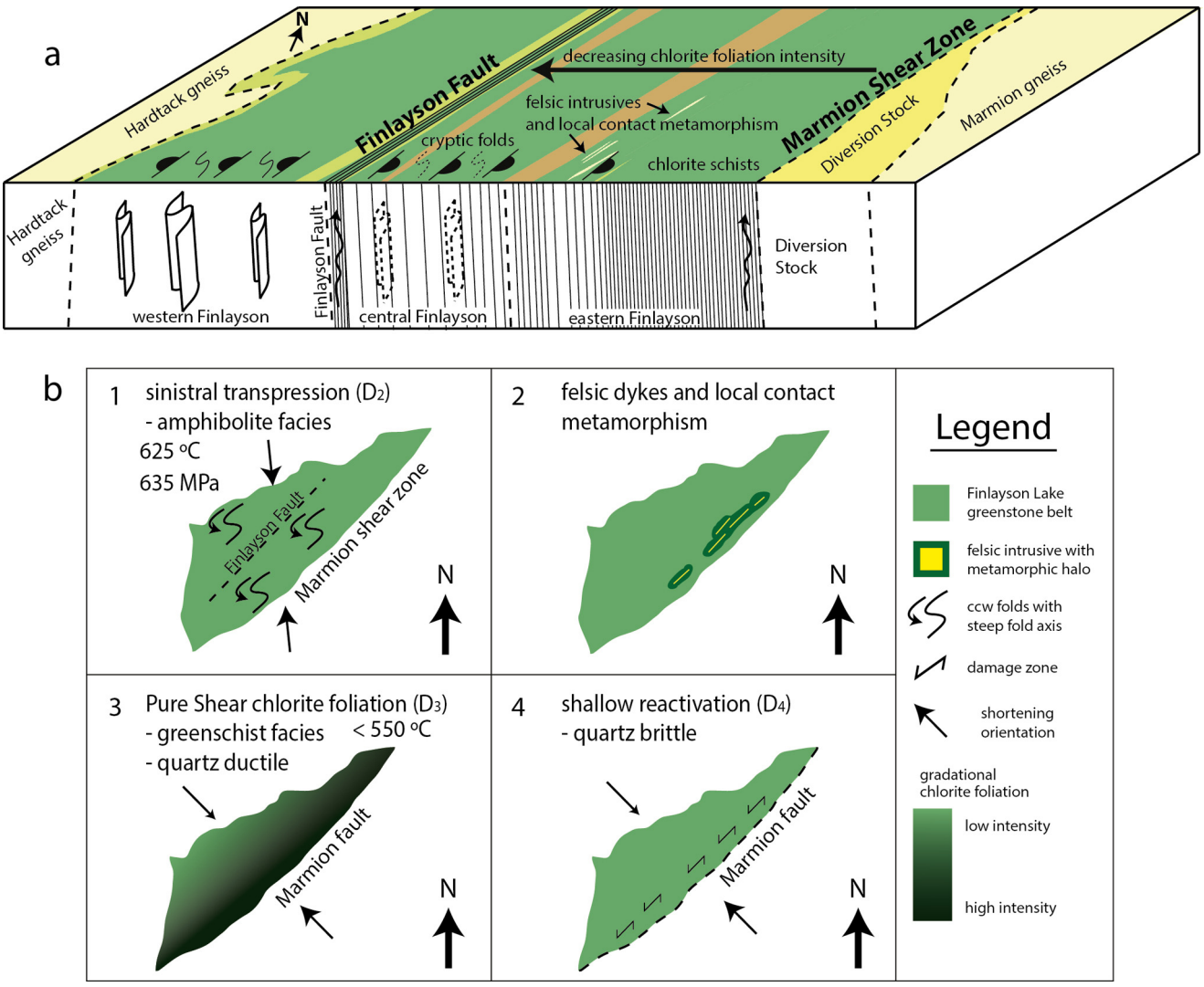

Fig. 8. (a) Sketch cross section of the Finlayson Lake greenstone belt. Density of solid lines represents intensity of retrogressive chlorite foliation. Steeply plunging folds in western and central portion of the section indicate observed sinistral transpression (solid outline) and cryptic folds overprinted by chlorite foliation (dashed outline). Oppositely facing pillow domains are separated by the Finlayson Fault. (b) Breakdown of the deformation history of the Finlayson belt. (1) Sinistral transpression with approximately north-south shortening and sinistral folds. (2) Local felsic dykes and contact metamorphic aureoles, preserving zones of pillow basalts within the chlorite schist domain. (3) Greenschist facies pure shear chlorite foliation, showing increasing intensity towards the eastern boundary and the Marmion Fault. (4) Sinistral and dextral reactivation of pre-existing structures in the eastern Finlayson belt during shallow NW-SE shortening.

1982; Kloppenburg et al., 2001). Although the tectonic implications are disputed, a common result from detailed structural studies in greenstone belts is a polydeformation history (de Wit, 1991; Peterson and Zaleski, 1999; Polat and Kerrich, 1999; Thomlinson et al., 1999; Kloppenburg et al., 2001; Lin, 2005; Kerrich and Polat, 2006; Lin and Beakhouse, 2013).

We emphasise here the complex and diverse tectonic histories recorded in Archaean greenstone belt terranes and that multiple kinematic interpretations are presented for single greenstone belts globally, similar to the previous work for the Finlayson Lake greenstone belt. By combining detailed field mapping with structural and kinematic data we are able to establish the deformation history of greenstone belts and test the different hypotheses that exist for individual terranes. The consistent structural and kinematic evidence from across the Finlayson Lake greenstone belt supports the presence of a single volcanic package with a common deformation history. We show that the greenstone belt records a polydeformation history with sub-horizontal shortening axes and that the eastern boundary was an active structure during compressive deformation and exhumation. Thermodynamic data from mineral analyses show that the shortening axis was horizontal to depths of 27–30 km (D_1). Sinistral transpression of the Finlayson belt continued along the exhumation path past 21 km depth for D_2 and followed by flattening during the D_3 greenschist facies and D_4 brittle regimes. The overall structural geometry of the greenstone belt is not consistent with a synform as proposed by Stone and Kamineni (1989), but rather related to a belt-scale anticline, the hingeline of which we interpret as the trace of the Finlayson Fault. Local reversals in palaeo way-up orientations within the Finlayson belt can be explained by counterclockwise folds and sinistral transpression kinematics during D_2. Measurements from the exposed eastern boundary show a steep slightly outward (southeast) dipping greenstone belt margin, in contrast to the inward-dipping basin-shaped structure that was interpreted from gravity studies (Gibb et al., 1988).

It is important to highlight that siliciclastic sediments and clasts of tonalite similar in age and composition to the 3.0 Ga Marmion gneisses are incorporated within the Finlayson belt (Stone, 2010, and this study). The age and structural relations between the Finlayson and exposed Marmion-equivalent

terranes rule out the possibility of crustal buoyancy contrasts required for diapiric juxtaposition. The pressure–temperature calculations for maximum burial at D_1 and peak metamorphism at D_2 show a geothermal gradient of 20 and 30 °C/km, respectively. This is significantly colder compared to geothermal gradients of 30–50 °C/km expected for greenstone-TTG terranes in the Archaean (e.g. Watson, 1978; Condie, 1984). The cold geothermal gradient from our calculated pressure–temperature path (Fig. 7) is typical for subduction-accretion models as suggested for other Archaean terranes (e.g. Kisters et al., 2012; Dziggel et al., 2014). The pressure–temperature path of the Finlayson belt shows a steep exhumation path along near-isothermal conditions forming a clockwise pressure–temperature path (Fig. 7). Clockwise pressure–temperature paths are common for modern continental collision and subduction settings (Ernst, 1988; Handy et al., 1999; Van Staal et al., 2008). A modern example in the Alpine subduction-accretion setting (the Ivrea crustal section), shows a multistage deformation history of prograde and peak metamorphism accompanying the dominant structural fabrics, followed by overprinting greenschist facies retrogression during exhumation (Handy et al., 1999).

The deformation fabrics in the Finlayson belt, specifically D_2 structures, have strong similarities to deformation fabrics described for the Schreiber-Hemlo greenstone belt in the Wawa subprovince, including steep fold axes that have been attributed to a transpressional setting (Polat and Kerrich, 1999; Kerrich and Polat, 2006). Polat and Kerrich (1999) interpret the tectonic setting of the Schreiber-Hemlo greenstone belt as a result of subduction-accretion. It is important when interpreting the palaeo-tectonic setting of Archaean rocks to account for the conditions of petrogenesis, deposition, deformation and metamorphism.

The lithologies of the Finlayson belt are comparable to any typical Archaean greenstone belt, containing abundant pillow basalts and massive basaltic lavas as the predominant lithologies together with siliciclastic siltstone, sandstones and conglomerates and chemical sediments followed by younger felsic intrusives. No komatiites have been observed in the Finlayson belt, but komatiites have been mapped in the adjacent Lumby Lake greenstone belt, which is of the same age. These lithologies have been argued to be typical of oceanic plateaus (e.g. Desrochers et al., 1993; Polat and Kerrich, 1999; Wang et al., 2013), where magmatic production is more volumetrically significant than sedimentation, and water depth is somewhat shallow.

Comparing Archaean greenstone belts to modern subduction-accretion settings based on lithologies is difficult, as the archetypal signature is the dominant sedimentary package, which are not observed in most greenstone belts. The depositional basins associated with Phanerozoic subduction settings are quite variable. Most trench deposition is characterised by voluminous, relatively immature clastic sediments, with minor volcanics and chemical sediments (e.g. Xiao et al., 2002; Ota et al., 2007). Tectonic mélanges, thought by many to be a structural signature of subduction, form most readily in subducting sediments (Moore et al., 1985). However, many active subduction zones have little or no sediment deposited in the trench, and the subducting pile is dominated by oceanic magmatic rocks and chemical sediments. Thin subducting sediments are correlated with narrow, intense shearing, so the voluminous tectono-sedimentary mélanges known from Phanerozoic accretionary wedges are not expected (c.f. Meneghini et al., 2009). Oceanic plate assemblages, subducted and then tectonically underplated, are preserved in the rock record (e.g. the Nicoya Ophiolite, Berrange and Thorpe, 1988; Vannucchi et al., 2006). This phenomenon may be favoured by thicker, more buoyant oceanic crust, even under modern conditions. Thus, a modern analog exists for developing an assemblage dominated by oceanic volcanism and minor sedimentation (oceanic plateau or proximal rift) and imposing a subduction-type metamorphic path on those rocks. The lithologies of the Finlayson belt do not discriminate between depositional settings (e.g. back arc, rift, oceanic plateau). Our observations, which focus on the detailed structural and metamorphic history of the Finlayson belt show similarities in structural and metamorphic evolution to modern subduction-accretion settings.

8. Conclusion

We have shown that the Finlayson Lake greenstone belt preserves a polydeformation history of at least four distinct events that follow a clockwise pressure–temperature path. The shortening axis remains horizontal throughout the deformation history, recording an older amphibolite facies sinistral transpression during peak metamorphism, which is followed by a retrogressive flattening and brittle faulting during exhumation. Our results are consistent with a subduction-accretion tectonic setting for the Finlayson Lake greenstone belt. Detailed kinematic and structural studies of greenstone belts worldwide show the importance of polydeformation histories with varied shortening orientation, often sub horizontal. Therefore, in order to correctly interpret the tectonic settings of greenstone-TTG terranes the details of the local and regional deformation histories need to be understood. In this study we show that by further defining the kinematics and deformation histories of Archaean terranes, the tectonic processes that juxtaposed supracrustal and crustal terranes can be tested. This is a necessary step before we can truly resolve the tectonic processes that resulted in all representative greenstone belt geometries globally and further our understanding of Early Earth processes.

Acknowledgements

This project was funded by Osisko Exploration Ltd. and the Natural Sciences and Engineering Research Council of Canada through a Collaborative Research and Development grant to Christie Rowe. Osisko provided us with field logistics and ongoing support throughout the study. We thank the reviewers and editor for their comments, which greatly strengthened the manuscript. A special thank you to Robert Wares, Anne Charland, Denis Villeneuve, Zoran Madon and many other Osisko employees for their discussions, interest and support. Especially, we would like to thank Denver Stone, who produced the regional maps and introduced us to the local geology and shared his thoughts and experience from many years of mapping. Thanks to Ben “Silky Chicken” Melosh for continued discussions and spell checks throughout this project, to Aeron Vaillancourt, Robert Borowski, Ian Carvalho-Campos and Kristyn Rodzinyak from McGill University for their assistance during field work and also Boswell Wing for introducing us to the area.

References

Anhaeusser, C., 1984. Structural Elements of Archaean Granite-Greenstone Terranes as Exemplified by the Barberton Mountain Land, Southern Africa. Precambrian Tectonics Illustrated, pp. 57–78.

Anhaeusser, C.R., Mason, R., Viljoen, M.J., Viljoen, R.P., 1969. A reappraisal of some aspects of Precambrian shield geology. Geol. Soc. Am. Bull. 80 (11), 2175–2200.

Bauer, R.L., Hudleston, P.J., Southwick, D.L., 1992. Deformation across the western Quetico subprovince and adjacent boundary regions in Minnesota. Can. J. Earth Sci. 29 (10), 2087–2103.

Berrange, J., Thorpe, R., 1988. The geology, geochemistry and emplacement of the Cretaceous–Tertiary ophiolitic Nicoya Complex of the Osa Peninsula, southern Costa Rica. Tectonophysics 147 (3), 193–220.

Borowski, R., 2013. Understanding the tectonics of Archean gneisses in the western Wabigoon terrane: evidence from the Dashwa Gneiss, Atikokan, Ontario. Master's thesis, McGill University.

Borradaile, G.J., Schwerdtner, W., 1984. Horizontal shortening of upward-facing greenstone structures in the southern Superior Province, Canadian Shield. Can. J. Earth Sci. 21 (5), 611–615.

Calvert, A.J., Sawyer, E.W., Davis, W.J., Ludden, J.N., 1995. Archean subduction inferred from seismic images of a mantle suture in the Superior Province. Nature 375, 670–674.
Card, K.D., 1990. A review of the Superior Province of the Canadian Shield, a product of Archean accretion. Precambrian Res. 48, 99–156.
Chardon, D., Choukroune, P., Jayananda, M., 1998. Sinking of the Dharwar Basin (South India): implications for Archean tectonics. Precambrian Res. 91, 15–39.
Collins, W.J., 1989. Polydiapirism of the Archean Mount Edgar Batholith, Pilbara Block, Western Australia. Precambrian Res. 43, 41–62.
Collins, W.J., Teyssier, C., 1990. Mount Edgar Batholith and Warrawoona Syncline. In: Ho, S.E., Glover, J.E., Myers, J.S., Muhling, J.R. (Eds.), Third International Archean Symposium, vol. 21. University of Western Australia, Perth, pp. 36–45.
Collins, W.J., Van Kranendonk, M.J., Teyssier, C., 1998. Partial convective overturn of Archean crust in the east Pilbara Craton, Western Australia: driving mechanisms and tectonic implications. J. Struct. Geol. 20 (9/10), 1405–1424.
Condie, K.C., 1984. Archean geotherms and supracrustal assemblages. Tectonophysics 105 (1), 29–41.
Connolly, J.A.D., 2005. Computation of phase equilibria by linear programming: a tool for geodynamic modeling and its application to subduction zone decarbonation. Earth Planet. Sci. Lett. 236, 524–541.
Davis, D.W., Jackson, M.C., 1988. Geochronology of the Lumby Lake greenstone belt: a 3 Ga complex within the Wabigoon subprovince, northwest Ontarop. Geol. Soc. Am. Bull. 100, 818–824.
de Wit, M.J., 1982. Gliding and overthrust nappe tectonics in the Barberton greenstone belt. J. Struct. Geol. 4 (2), 117–136.
de Wit, M.J., 1991. Archaean greenstone belt tectonism and basin development: some insights from the Barberton and Pietersburg greenstone belts, Kaapvaal Craton, South Africa. J. Afr. Earth Sci. (Middle East) 13 (1), 45–63.
de Wit, M.J., 1998. On Archean granites, greenstones, cratons and tectonics: does the evidence demand a verdict? Precambrian Res. 91, 181–226.
Desrochers, J.-P., Hubert, C., Ludden, J.N., Pilote, P., 1993. Accretion of Archean oceanic plateau fragments in the Abitibi, greenstone belt, Canada. Geology 21 (5), 451–454.
Diener, J.F.A., Powell, R., 2012. Revised activity-composition models for clinopyroxene and amphibole. J. Metamorphic Geol. 30, 131–142.
Diener, J.F.A., Powell, R., White, R.W., Holland, T.J.B., 2007. A new thermodynamic model for clino- and orthoamphiboles in the system Na_2O-CaO-FeO-MgO-Al_2O_3-SiO_2-H_2O-O. J. Metamorphic Geol. 25, 631–656.
Dziggel, A., Diener, J.F.A., Kolb, J., Kokfelt, T.F., 2014. Metamorphic record of accretionary processes during the Neoarchaean: the Nuuk region, southern West Greenland. Precambrian Res. 242, 22–38.
Ernst, W., 1988. Tectonic history of subduction zones inferred from retrograde blueschist PT paths. Geology 16 (12), 1081–1084.
Fyson, W.K., 1978. Structures induced by granite diapirs in the Archaean greenstone belt at Yellowknife, Canada: implications for Archaean geotectonics: a discussion. J. Geol. 86 (6), 767–769.
Gibb, R.A., Nagy, D., Coderre, J., Fogarasi, A., Thomas, M.D., 1988. Gravity surveys and interpretation, Eye-Dashwa lakes pluton, Atikokan (RA 4), Ontario. Tech. Rep., Geological Survey of Canada.
Hamilton, W.B., 1998. Archean magmatism and deformation were not products of plate tectonics. Precambrian Res. 91, 143–179.
Handy, M., Franz, L., Heller, F., Janott, B., Zurbriggen, R., 1999. Multistage accretion and exhumation of the continental crust (Ivrea crustal section, Italy and Switzerland). Tectonics 18 (6), 1154–1177.
Holland, T., Baker, J., Powell, R., 1998. Mixing properties and activity-composition and relationships of chlorites in the system MgO-FeO-Al_2O_3-SiO_2-H_2O. Eur. J. Mineral. 10 (3), 395–406.
Holland, T., Blundy, J., 1994. Non-ideal interactions in calcic amphiboles and their bearing on amphibole-plagioclase thermometry. Contrib. Mineral. Petrol. 116 (4), 433–447.
Holland, T., Powell, R., 1996. Thermodynamics of order-disorder in minerals: II. Symmetric formalism applied to solid solutions. Am. Mineral. 81 (11), 1425–1437.
Holland, T.J.B., Powell, R., 1998. An internally-consistent thermodynamic dataset for phases of petrological interest. J. Metamorphic Geol. 16, 309–344.
Kerrich, R., Polat, A., 2006. Archean greenstone-tonalite duality: thermochemical mantle convection models or plate tectonics in the early Earth global dynamics? Tectonophysics 415 (1), 141–165.
Kisters, A.F., van Hinsberg, V.J., Szilas, K., 2012. Geology of an Archaean accretionary complex – the structural record of burial and return flow in the Tartoq Group of South West Greenland. Precambrian Res. 220, 107–122.
Kloppenburg, A., White, S.H., Zegers, T.E., 2001. Structural evolution of the Warrawoona Greenstone Belt and adjoining granitoid complexes, Pilbara Craton, Australia: implications for Archean tectonic processes. Precambrian Res. 112, 107–147.
Kretz, R., 1983. Symbols for rock-forming minerals. Am. Mineral. 68, 277–279.
Kusky, T., Li, X., Wang, Z., Fu, J., Ze, L., Zhu, P., 2014. Are Wilson cycles preserved in Archean Cratons? A comparison of the North China and Slave Cratons. Can. J. Earth Sci. 51, 297–311.
Kusky, T.M., Vearncombe, J.R., 1997. Structural Aspects. In: de Wit, M.J., Ashwal, L.D. (Eds.), Greenstone Belts. Oxford University Press, pp. 91–124 (chapter 2.3).
Lin, S., 2005. Synchronous vertical and horizontal tectonism in the Neoarchean: kinematic evidence from a synclinal keel in the northwestern Superior craton, Canada. Precambrian Res. 139, 181–194.
Lin, S., Beakhouse, G.P., 2013. Synchronous vertical and horizontal tectonism at late stages of Archean cratonization and genesis of Hemlo gold deposit, Superior craton, Ontario, Canada. Geology 41 (3), 359–362.
Lin, S., Percival, J.A., Skulski, T., 1996. Structural constraints on the tectonic evolution of a late Archean greenstone belt in the northeastern Superior Province, northern Quebec (Canada). Tectonophysics 265, 151–167.
Marshak, S., Alkmim, F., 2012. Contrasting mechanisms for gneiss-dome formation in Precambrian dome-and-keel provinces: a record of evolving styles of crustal flows. In: Geological Society of America Abstract with Programs, vol. 44, Charlotte Convention Center 207D, p. 70.
Marshak, S., Alkmim, F., Jordt-Evangelista, H., 1992. Proterozoic crustal extension and the generation of dome-and-keel structure in an Archaean granite-greenstone terrane. Nature 357, 491–493.
Meneghini, F., Marroni, M., Moore, J., Pandolfi, L., Rowe, C., 2009. The processes of underthrusting and underplating in the geologic record: structural diversity between the Franciscan Complex (California), the Kodiak Complex (Alaska) and the Internal Ligurian Units (Italy). Geol. J. 44 (2), 126–152.
Minnett, R.C.A., Anhaeusser, R.C., 1992. Gravitational and diapiric structural history of the eastern portion of the Archaean Murchison greenstone belt, South Africa. J. Afr. Earth Sci. 15 (3/4), 429–440.
Moore, J.C., Cowan, D.S., Karig, D.E., 1985. Structural styles and deformation fabrics of accretionary complexes. Geology 13 (1), 77–79.
Musacchio, G., White, D., Asudeh, I., Thomson, C., 2004. Lithospheric structure and composition of the Archean western Superior Province from seismic refraction/wide-angle reflection and gravity modeling. J. Geophys. Res.: Solid Earth (1978–2012), 109.
Newton, R.C., Wood, B.J., Kleppa, O.J., 1981. Thermochemistry of silicate solid solutions. Bull. Mineral. 104, 162–171.
Ota, T., Utsunomiya, A., Uchio, Y., Isozaki, Y., Buslov, M.M., Ishikawa, A., Maruyama, S., Kitajima, K., Kaneko, Y., Yamamoto, H., et al., 2007. Geology of the Gorny Altai subduction-accretion complex, southern Siberia: tectonic evolution of an Ediacaran-Cambrian intra-oceanic arc-trench system. J. Asian Earth Sci. 30 (5), 666–695.
Parmenter, A.C., Lin, S., Corkery, M.T., 2006. Structural evolution of the Cross Lake greenstone belt in the northwestern Superior Province, Manitoba: implications for relationship between vertical and horizontal tectonism. Can. J. Earth Sci. 43 (7), 767–787.
Percival, J.A., 1989. A regional perspective of the Quetico metasedimentary belt, Superior Province, Canada. Can. J. Earth Sci. 26 (4), 677–693.
Percival, J.A., 2007a. Eo- to Mesoarchean terranes of the Superior Province and their tectonic context. In: Van Kranendonk, M.J., Smithies, R.H., Bennet, V.C. (Eds.), In: Earth's Oldest Rocks. Developments in Precambrian Geology, vol. 15, pp. 1065–1085.
Percival, J.A., 2007b. Geology and metallogeny of the Superior Province, Canada. In: Goodfellow, W.D. (Ed.), Mineral Deposits of Canada: A Synthesis of Major Deposit-Types, District Metallogeny, the Evolution of Geology Provinces, and Exploration Methods. Geological Association of Canada, Mineral Deposits Devision, Special Publication No. 5, pp. 903–928.
Percival, J.A., Helmstaedt, H., 2004. Insights on Archean continent-ocean assembly, western Superior Province, from new structural, geochemical and geochronological observations: introduction and summary. Precambrian Res. 132, 209–212.
Percival, J.A., McNicoll, V., Brown, J.L., Whalen, J.B., 2004. Convergent margin tectonics, central Wabigoon subprovince, Superior Province, Canada. Precambrian Res. 132, 213–244.
Percival, J.A., Sanborn-Barrie, M., Skulski, T., Stott, G.M., Helmstaedt, H., White, D.J., 2006. Tectonic evolution of the western Superior Province from NATMAP and Lithoprobe studies. Can. J. Earth Sci. 43, 1085–1117.
Percival, J.A., Williams, H.R., 1989. Late Archean Quetico accretionary complex, Superior province, Canada. Geology 17 (1), 23–25.
Peschler, A., Benn, K., Roest, W., 2004. Insights on Archean continental geodynamics from gravity modelling of granite-greenstone terranes. J. Geodyn. 38 (2), 185–207.
Peterson, V.L., Zaleski, E., 1999. Structural history of the Manitouwadge greenstone belt and its volcanogenic Cu–Zn massive sulphide deposits, Wawa subprovince, south-central Superior Province. Can. J. Earth Sci. 36 (4), 605–625.
Polat, A., Kerrich, R., 1999. Formation of an Archean tectonic mélange in the Schreiber-Hemlo greenstone belt, Superior Province, Canada: implications for Archean subduction-accretion process. Tectonics 18 (5), 733–755.
Polat, A., Kerrich, R., 2001. Geodynamic processes, continental growth, and mantle evolution recorded in late Archean greenstone belts of the southern Superior Province, Canada. Precambrian Res. 112 (1), 5–25.
Polat, A., Kerrich, R., Wyman, D., 1998. The late Archean Schreiber-Hemlo and White River-Dayohessarah greenstone belts, Superior Province: collages of oceanic plateaus, oceanic arcs, and subduction-accretion complexes. Tectonophysics 289 (4), 295–326.
Ranganai, R.T., 2012. Gravity and aeromagnetic studies of the Filabusi greenstone belt, Zimbabwe Craton: regional and geotectonic implications. Int. J. Geosci. 3 (5), 1048–1064.
Robin, C.M.I., Bailey, R.C., 2009. Simultaneous generation of Archean crust and subcratonic roots by vertical tectonics. Geology 37 (6), 523–526.
Schwerdtner, W.M., 1982. Salt stocks as natural analogues of Archean gneiss diapirs. Geol. Rundsch. 71 (1), 370–379.
Schwerdtner, W.M., 1984. Foliation patterns in lagre gneiss bodies of the Archean Wabigoon Subprovince, southern Canadian shield. J. Geodyn. 1, 313–337.
Schwerdtner, W.M., 1990. Structural tests of diapir hypotheses in Archean crust of Ontario. Can. J. Earth Sci. 27, 387–402.

Schwerdtner, W.M., Stone, D., Osadetz, K., Morgan, J., Stott, G.M., 1979. Granitoid complexes and the Archean tectonic record in the southern part of northwestern Ontario. Can. J. Earth Sci. 16, 1965–1977.
Sleep, N.H., Windley, B.F., 1982. Archean plate tectonics: constraints and inferences. J. Geol. 90 (4), 363–379.
Stettler, E., Du Plessis, J., De Beer, J., 1988. The structure of the Pietersburg greenstone belt, South Africa, as derived from geophysics. S. Afr. J. Geol. 91 (2), 292–303.
Stettler, E.H., de Beer, J.H., Eberle, D., Ludden, J., Mareschal, M., 1997. Greenstone-belt boundaries, surrounding-rock terrains, and their interrelations: geophysics and deep structure. In: de Wit, M.J., Ashwal, L.D. (Eds.), Greenstone Belts. Oxford University Press, pp. 339–375 (chapter 4.1).
Stone, D., 2008. Precambrian geology, Atikokan Area, Preliminary Map P. 3349-Revised. Tech. Rep., Ontario Geological Survey.
Stone, D., 2010. Precambrian geology of the central Wabigoon subprovince area, northwest Ontario. Tech. Rep., Open File Report 5422, Ontario Geological Survey.
Stone, D., Kamineni, D.C., 1989. Geology, Atikokan Area, Ontario, Map 1666, Scale 1:50 000. Tech. Rep., Geological Survey of Canada.
Stone, D., Kamineni, D.C., Jackson, M.C., 1992. Precambrian Geology of the Atikokan Area, Northwestern Ontario. Tech. Rep. Bulletin 405, Geological Survey of Canada.
Thomlinson, K.Y., Davis, D.W., Stone, D., Hart, T.R., 2003. U–Pb age and Nd isotopic evidence for Archean terrane development and crustal recycling in the south-central Wabigoon subprovince, Canada. Contrib. Mineral. Petrol. 144, 684–702.
Thomlinson, K.Y., Hughes, D.J., Thurston, P.C., Hall, R.P., 1999. Plume magmatism and crustal growth at 2.9 to 3.0 Ga in the Steep Rock and Lumby Lake area, Western Superior Province. Lithos 46, 103–136.
Tomlinson, K.Y., Stone, D., Hattori, K.H., 2004. Basement terranes and crustal recycling in the western Superior Province: Nd isotopic character of granitoid and felsic volcanic rocks in the Wabigoon subprovince, N. Ontario, Canada. Precambrian Res. 132, 245–274.
van Hunen, J., van Keken, P.E., Hynes, A., Davies, G.F., 2008. Tectonics of early Earth: some geodynamic considerations. In: Condie, K.C., Pease, V. (Eds.), When Did Plate Tectonics Begin on Planet Earth?, Geological Society of America Special Paper, vol. 440. , pp. 157–171.
Van Kranendonk, M.J., Collins, W.J., Hickman, A., Pawlay, M.J., 2004. Critical tests of vertical vs. horizontal tectonic models for the Archean East Pilbara granite-greenstone terrane, Pilbara Craton, Western Australia. Precambrian Res. 131, 173–211.
Van Staal, C., Currie, K., Rowbotham, G., Rogers, N., Goodfellow, W., 2008. Pressure–temperature paths and exhumation of Late Ordovician-Early Silurian blueschists and associated metamorphic nappes of the Salinic Brunswick subduction complex, northern Appalachians. Geol. Soc. Am. Bull. 120 (11–12), 1455–1477.
Vannucchi, P., Fisher, D.M., Bier, S., Gardner, T.W., 2006. From seamount accretion to tectonic erosion: formation of Osa Mélange and the effects of Cocos Ridge subduction in southern Costa Rica. Tectonics 25 (2).
Wang, J., Kusky, T., Polat, A., Wang, L., Deng, H., Wang, S., 2013. A late Archean tectonic mélange in the Central Orogenic Belt, North China Craton. Tectonophysics 608, 929–946.
Watson, J.V., 1978. Precambrian thermal regimes. Philos. Trans. R. Soc. Lond. Ser. A: Math. Phys. Sci. 288 (1355), 431–440.
Whalen, J.B., Percival, J.A., McNICOLL, V.J., Longstaffe, F.J., 2002. A mainly crustal origin for tonalitic granitoid rocks, superior province, Canada: implications for late Archean Tectonomagmatic processes. J. Petrol. 43 (8), 1551–1570.
White, D., Musacchio, G., Helmstaedt, H., Harrap, R., Thurston, P., Van der Velden, A., Hall, K., 2003. Images of a lower-crustal oceanic slab: direct evidence for tectonic accretion in the Archean western Superior province. Geology 31 (11), 997–1000.
White, R., Powell, R., Holland, T., 2007. Progress relating to calculation of partial melting equilibria for metapelites. J. Metamorphic Geol. 25 (5), 511–527.
White, R., Powell, R., Holland, T., Worley, B., 2000. The effect of TiO∼2 and Fe∼2O∼3 on metapelitic assemblages at greenschist and amphibolite facies conditions: mineral equilibria calculations in the system K∼2O-FeO-MgO-Al∼2O∼3-SiO∼2-H∼2O-TiO∼2-Fe∼2O∼3. J. Metamorphic Geol. 18 (5), 497–512.
Wilks, M., Nisbet, E., 1988. Stratigraphy of the Steep Rock Group, northwest Ontario: a major Archaean unconformity and Archaean stromatolites. Can. J. Earth Sci. 25 (3), 370–391.
Williams, H.R., 1990. Subprovince accretion tectonics in the south-central Superior Province. Can. J. Earth Sci. 27 (4), 570–581.
Xiao, W.J., Windley, B.F., Chen, H.L., Zhang, G.C., Li, J.L., 2002. Carboniferous-Triassic subduction and accretion in the western Kunlun, China: implications for the collisional and accretionary tectonics of the northern Tibetan Plateau. Geology 30 (4), 295–298.
Zegers, T.E., van Keken, P.E., 2001. Middle Archean continent formation by crustal delamination. Geology 29 (12), 1083–1086.